Colloidal aggregation with mobile impurities

A. AlSunaidi,[1] M. Lach-hab,[1] Estela Blaisten-Barojas,[1,*] and Agustín E. González[2,†]
[1]*School of Computational Sciences, George Mason University, Fairfax, Virginia 22030*
[2]*Centro de Ciencias Físicas, Universidad Nacional Autónoma de México, Apartado Postal 48-3, Cuernavaca, Morelos 62251, México*
(Received 9 December 1999)

The structure and aggregation kinetics of diffusion-limited cluster-cluster three-dimensional monomeric aggregates and gels is investigated as a function of the molar fraction of two types of impurity. In one case the impurities are allowed to aggregate among themselves whereas in the other the impurities are mobile monomers that remain as such during the whole aggregation process. Computer simulations are performed on a simple cubic lattice for which the functionality of the aggregating particles is effectively 6. The first type of impurity shows a decrease in the fractal dimension when compared to that of a one component system at the same concentration. As a consequence of this decrease, the gelation concentration is lowered. At higher concentrations a gelling to nongelling transition was observed. In the nongelling regime the colloidal aggregates are kept apart by the impurity clusters, developing a local ordering. For the monomeric type of impurity, at large impurity molar fractions, a nonstructured nongelling phase appears at high enough concentration, in which the colloidal aggregates are kept apart by the sea of mobile impurities that inhibits the formation of a gel. Smaller molar fractions of mobile monomeric impurities strongly affect both the fractal dimension and the kinetics of the aggregating colloid.

PACS number(s): 61.43.Hv, 82.70.Dd, 82.70.Gg, 05.10.Ln

I. INTRODUCTION

The effects of impurities, filler, or secondary particles on the properties of aggregating systems have been investigated experimentally for a variety of systems. For example, polyelectrolytes were found to play the role of impurities in crystallizing systems [1], affecting the nucleation, growth and aggregation, and phase transformations. Macromolecular impurities affect protein solubility and crystallizability. Even a small amount of protein impurity can impede growth step propagation and these impurities play a role in the formation of structural/compositional inhomogeneities [2–4]. Impurities were also found to affect the dynamics of micellization [5], rheology of gels [6], and morphology of phospholipid monolayers [7].

Several studies have been performed to correlate these structural and kinetic changes with both the concentration of impurities and the type of interactions between them and the host particles. Experiments by van Vliet [8] show that the interaction of emulsion droplets with casein micelles results in an increase in the storage modulus of the gel. However, when the droplets did not interact, the storage modulus decreased monotonically with the concentration of filler particles. A recent experimental study on gold/silica gel [9] shows no significant change in the structure of the silica gel due to the presence of a low molar fraction of small colloidal gold particles and a decrease in the average pore size of the silica gel when the gold colloidal particles are large.

Concerning numerical investigation of the effect of impurities, studies of the effect of mobile impurities on an advancing solidification front [10,11] are available. The growth model in these studies is local and does not have the kinetic component included in diffusion-limited cluster-cluster aggregation (DLCA). An epidemic Eden cluster on square [10] and cubic lattices [11] grows in a liquid phase containing a molar fraction x of mobile impurities. The impurities are pushed by the advancing front due to repulsive forces. This system exhibits a percolationlike transition at x_c, displaying a continuous nonstopping growth below x_c and finite clusters due to a complete hindrance of growth above x_c. The value of x_c is larger in three dimensions (3D) than in (2D) and is larger than the critical molar fraction found for the corresponding epidemic model with static impurities. At x_c the clusters and internal patterns are found to have a fractal perimeter with the same dimension as that of classical percolation [12].

Recently [13], we have modified the diffusion-limited cluster-cluster aggregation algorithm to take into account the existence of two types of colloidal particle interacting attractively in the aggregating system. There are two aggregation regimes depending on the molar fraction x of one type of particle. When $x<0.2$ a nongelling regime is attained and the simulation ends with a sol composed of saturated oligomers. As x decreases from 0.5 to 0.2, the system shows a crossover from DLCA aggregates equivalent to those of the one-monomer system at that concentration [14] to aggregates obtained in reaction-limited cluster-cluster aggregation.

In this paper we study the effect of mobile impurities on the structure, kinetics, and gelation of a colloidal system performing a diffusion-limited cluster-cluster aggregation. Impurities are defined as particles that may or may not interact within themselves but do not interact with the colloidal system except through excluded volume interactions. We consider two types of impurities: aggregating impurities that could form fractal clusters (model 1) and unreactive monomeric impurities (model 2). In both cases the impurity particles do not react with the aggregating colloid. The two types of impurity belong to different classes of obstacles (fractal and nonfractal) that have shown different behavior in

*Electronic address: eblaiste@gmu.edu
†Electronic address: agus@fis.unam.mx

lateral diffusion measurements of submicroscopic domain structures [15]. In fact, it is not only the geometry of the impurity particles that affects the aggregation process, but also their size and mobility. We study here the aggregate morphology and kinetics as a function of the molar fraction of impurities x and look for a critical molar fraction x_c where a blocking transition occurs (similar to that found in the dynamic Eden model [10,11]). A comparison of results to those of DLCA of a one-monomer system [14] is given for the two models.

This paper is organized as follows. A detailed description of the models and the computer algorithm is given in Sec. II. The dependence on the total concentration of the system ϕ and on the relative concentration of the impurities of the structure and kinetics is presented in Secs. III and IV, respectively. Section V describes the effect of the impurities on the threshold to gelation and the gelation properties of the system. Concluding remarks close this work in Sec. VI.

II. MODEL AND METHODS

Two models of DLCA with impurities are described in this section. The B particles are colloidal DLC aggregating monomers that diffuse in a medium containing impurities represented by particles A. The colloidal particles and the impurities are assumed to be of equal size. Both the host B particles and the impurities diffuse on a 3D cubic lattice; thus their functionality is $f=6$ (number of nearest neighbors). The host particles perform irreversible cluster-cluster aggregation with sticking probabilities $P_{BB}=1$ and do not interact with the impurities such that $P_{AB}=0$. In model 1 the impurities also diffuse under DLCA with sticking probability $P_{AA}=1$, indicating that impurity particles are allowed to interact attractively with each other (their functionality is also $f=6$). As the impurity clusters grow in size, obstacles are formed that affect the growth of the host clusters of type B. This structural effect will have an impact on the kinetics especially when the average distance between the clusters is short. In model 2 the impurities diffuse without aggregating and $P_{AA}=0$. In this model impurities are unreactive particles whose size does not change with time. Therefore, as the host B clusters grow larger, the kinetics is dominated by the movement of the impurity particles which are light. This fact not only slows down the growth of the B clusters, but also restricts their available growth space. As a consequence the structure of the B clusters is affected.

All simulations are carried out in cubic computational boxes of length L and periodic boundary conditions are used. When the simulation is started, the system is a mixture of a molar fraction x (or N_A) of impurity particles and $(1-x)$ (or N_B) of colloidal host particles, either one of them occupying random cells of the cubic lattice. The molar fraction of the impurities is $x=N_A/(N_A+N_B)$. The number of occupied cells is determined by the volume fraction (concentration) $\phi=(N_A+N_B)/V$, where $V=L^3$ is the volume of the computational box. The concentration ϕ and molar fraction x are related through the relative concentrations $\phi_B=(1-x)\phi=N_B/V$ and $\phi_A=x\phi=N_A/V$. The total number of particles $N=N_A+N_B$ is $\approx 470\,000$ for all simulations at three different concentrations: $\phi=0.01$, 0.03, and 0.05, corresponding to computational boxes of side $L=360$, 250 and 210, respectively.

Initially the simulation box contains unaggregated particles of type A and type B. The time counter starts by randomly picking a particle, incrementing the time by the inverse of the number of clusters in the system (which at the beginning is $N_c=N_A+N_B$), and moving at random the selected particle by one unit cell. The motion of the particles is a random walk simulating their Brownian motion caused by the thermal fluctuations in the solvent. If a particle i attempts to occupy the position of a nearest-neighbor particle j, then the two particles stick (or not) with probability $P_{ij}=1$ or 0. In model 1, $P_{ij}=1$ if i and j are either two colloidal particles or two impurities, whereas $P_{ij}=0$ if one particle is a colloidal particle and the other is an impurity. In model 2, $P_{ij}=1$ only if i and j are two colloidal particles and equals zero otherwise.

At intermediate times the system contains clusters of different sizes and the aggregation continues by selecting at random a cluster of type A or B and size s. A size-dependent diffusion coefficient of the selected cluster is calculated as $D(s)\sim 1/R_g$, where R_g is the radius of gyration of that cluster. The time is then incremented by $1/N_c$, where N_c is the number of clusters in the system at that particular time. The selected cluster is allowed to move in a random direction by one lattice unit only if a random number X uniformly distributed in the range $0<X<1$ satisfies the condition $X<D(s)/D(1)$. The move will take place if no particle in the selected cluster overlaps cells occupied by another cluster. If it does, then the two clusters either stick permanently if $P_{ij}=1$ or remain side by side if $P_{ij}=0$, where i and j refer to the type of particles at contact. For the structural and kinetic calculations the aggregation process terminates when a floc forms, just before gelation where a spanning cluster is about to form. To determine the percolation threshold (or gelation threshold), the simulation is continued until no change in the number of clusters N_c occurs for a specified length of time. A gel is obtained when a cluster spans the computational box. This cluster is then fixed.

Several quantities are calculated during the aggregation process. For the purpose of calculating the fractal dimension d_f, the cluster radii of gyration, $R_g^2=(1/s)\Sigma_i(r_i-r_0)^2$, are calculated every time a new cluster is formed during the aggregation process. Here, s is the number of monomers in the cluster (mass), r_i is the position of the ith monomer, and r_0 is the cluster center of mass. Other monitored quantities are the moments of the cluster distribution function $N_s(t)$, such as the mean number of clusters $N_c(t)=\Sigma_s N_s(t)$ and the weight-average cluster size $S_w(t)=\Sigma_s s^2 N_s(t)/\Sigma_s s N_s(t)$, where the sums run over finite (nonspanning) clusters. Whenever a gel is formed, the gel fraction G is calculated as

$$G=\frac{(\text{number of particles belonging to the spanning cluster})}{(\text{total number of particles})}. \tag{1}$$

These properties are averaged over 50 simulations. Distances and time are reported in dimensionless units.

TABLE I. Slopes of the $\log\sigma_p$ vs $\log\sigma_q$ plots for different values of p and q at $\phi=0.01$ and 0.05 for model 1 and at $\phi=0.01$ for model 2. Only clusters containing more than 20 monomers were considered.

		Model 1				Model 2	
		$\phi=0.01$		$\phi=0.05$		$\phi=0.01$	
p	q	$x=0.3$	$x=0.7$	$x=0.3$	$x=0.7$	$x=0.1$	$x=0.5$
3	2	1.48±0.02	1.49±0.01	1.49±0.02	1.52±0.02	1.50±0.02	1.47±0.03
4	2	1.96±0.04	1.97±0.03	1.97±0.04	2.04±0.04	2.01±0.03	1.92±0.07
5	2	2.44±0.08	2.46±0.04	2.44±0.08	2.56±0.06	2.52±0.06	2.38±0.11
4	3	1.32±0.02	1.33±0.01	1.33±0.01	1.34±0.01	1.34±0.02	1.31±0.02
5	3	1.65±0.03	1.66±0.01	1.65±0.03	1.69±0.02	1.68±0.02	1.63±0.02
5	4	1.24±0.01	1.25±0.01	1.25±0.01	1.24±0.01	1.26±0.01	1.24±0.01

III. FRACTAL DIMENSION

The degree of compactness or ramification of a statistically self-similar cluster is measured by its fractal dimension d_f. To study the self-similarity of the clusters, the method based on the moments of the distribution of the cluster radii of gyration [16–18] was used. In this method the distribution of the cluster radii of gyration is generated for clusters of sizes larger than $s=20$ collected from the 50 simulations at each value of ϕ and each value of x. The moments of this distribution are defined as

$$\sigma_p(R_{g_i})=\frac{1}{n_i}\sum_{s=1}^{n_i}|R_{g_{i_s}}-\langle R_g\rangle|^p, \qquad (2)$$

where n_i is the number of clusters in the ith bin and $\langle R_g\rangle$ is the mean radius of gyration in that bin. Note that $\sigma_p \sim N_i^{p/d_f}$ if $R_{g_{i_s}}\sim N_{i_s}^{1/d_f}$. Therefore, if the system is characterized by one fractal dimension, then the ratio of $\ln(\sigma_p)$ to $\ln(\sigma_q)$ should be equal to p/q for all bins. A deviation from this value indicates multifractality. Our results for the two models are shown in Table I for different mole fractions x. As seen from the table, the calculated ratios $\ln(\sigma_p)/\ln(\sigma_q)$ are indeed equal to p/q. The uncertainties listed in the table correspond to twice the standard deviation. From this analysis we conclude that the clusters are self-similar at the concentrations considered in this study.

Once it is proved that the clusters in the two models are self-similar, the fractal dimension d_f is obtained from the mass-size relationship $N\sim R_g^{d_f}$. To avoid large fluctuations and in order to take the asymptotic limit of large clusters, only clusters containing more than 20 monomers in the 50 simulations were retained in the determination of d_f. In model 1, where the impurities aggregate, the dependence of the fractal dimension of the colloidal clusters B on their relative concentration ϕ_B and for three different concentrations of the whole system ϕ is shown in Fig. 1. Each point at a given concentration in Fig. 1(a) corresponds to a different value of x, the molar fraction of impurities present in the bath: 0.05, 0.1, 0.2, . . . ,0.9. For comparison, the dotted line corresponds to the dependence of the fractal dimension on concentration in the one-component system (OCS) [14]: $d_f=1.797+0.913\phi^{0.507}$. Notice that for the $\phi=0.01$ case, the fractal dimension of model 1 follows the OCS closely except at high x. For $\phi=0.03$ and 0.05, the fractal dimension approaches the OCS value as $x\to1$ and $x\to0$. In Fig. 1(b) these results are presented differently, indicating the dependence of d_f on the amount of impurities present, x. It is clear that at the same molar fraction of impurities there is an increase in d_f with total concentration due to an interpenetration of the colliding clusters [14]. There is a trend shown in

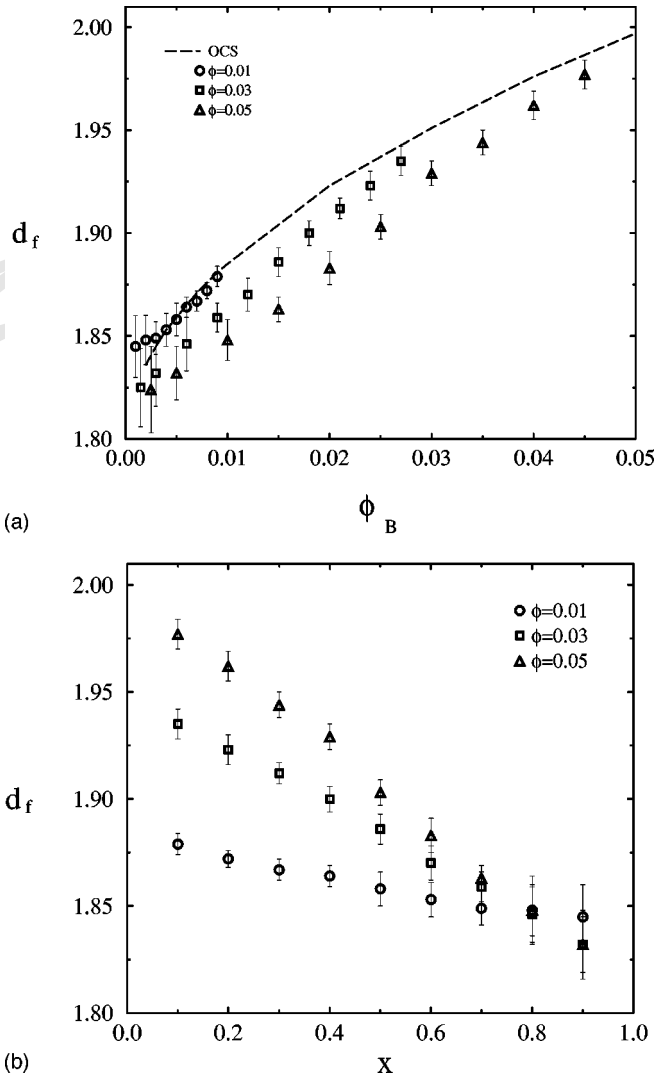

FIG. 1. Model 1. Fractal dimension at three concentrations $\phi=0.01$ (circles), 0.03 (squares), and 0.05 (triangles), (a) as a function of the relative concentration ϕ_B; (b) as a function of the impurity molar fraction x. The dotted line refers to the one component system.

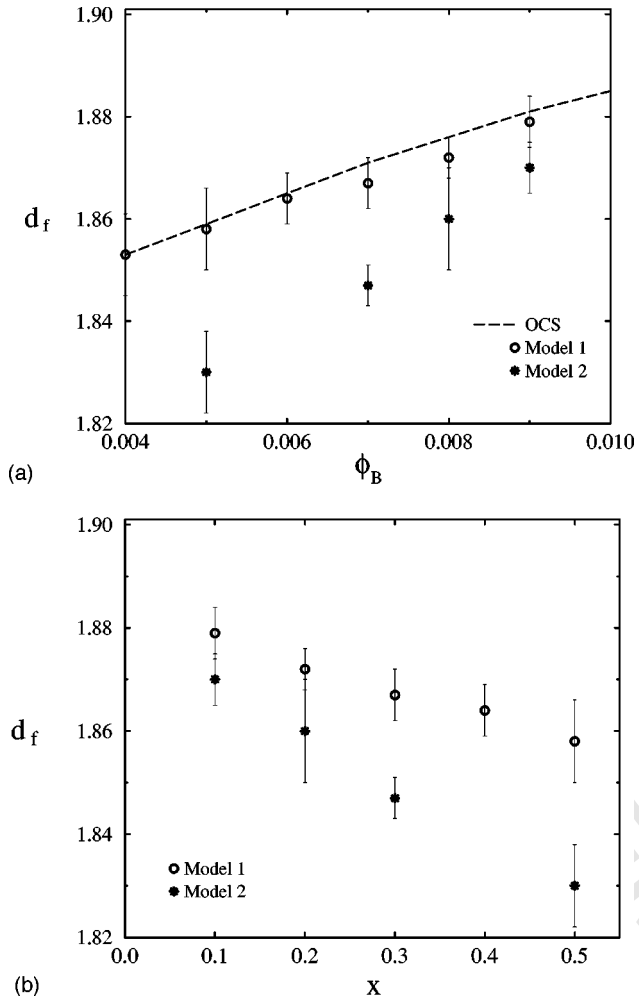

FIG. 2. Model 2. Fractal dimension at $\phi=0.01$ (asterisks) as compared to that of model 1 (circles), (a) as a function of the relative concentration ϕ_B; (b) as a function of the impurity molar fraction x. The dotted line refers to the one-component system.

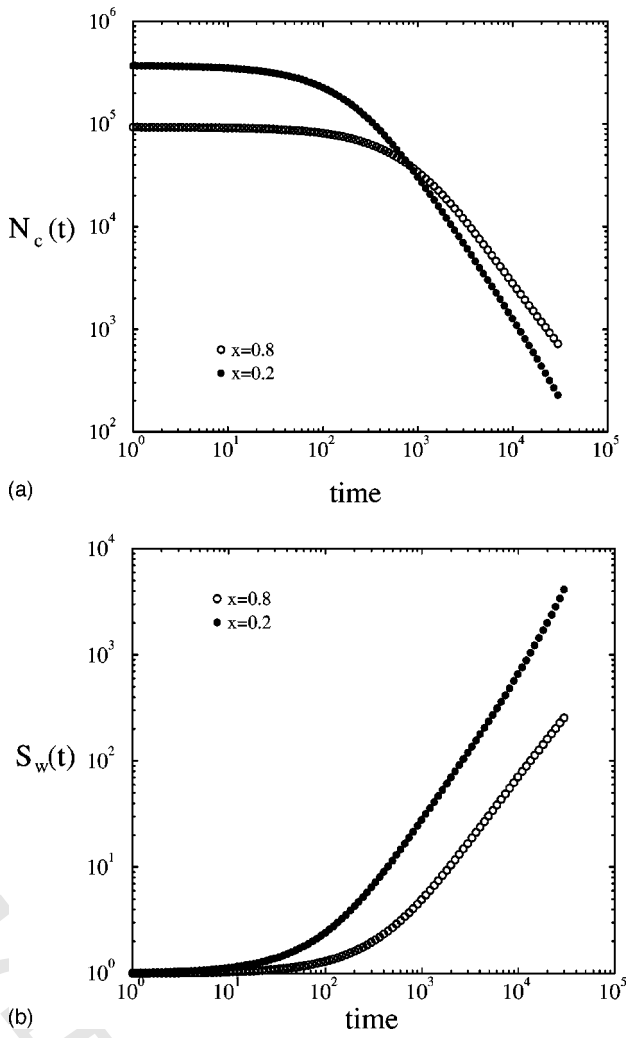

FIG. 3. Model 1: (a) Mean number of clusters $N_c(t)$ as a function of time. (b) Weight-average cluster size $S_w(t)$ as a function of time. Both plots are for $\phi=0.01$ and impurity molar fractions $x=0.2$ (black dots) and $x=0.8$ (circles).

Fig. 1(a), however, indicating that for more concentrated systems the fractal dimension of the colloidal particles is smaller than in the equivalent OCS. As the concentration increases the growing impurity clusters act as obstacles to the colloidal clusters, preventing the large colloidal clusters from growing homogeneously in space. Because the accretion of the large clusters in this model is not homogeneous, slightly more elongated and therefore less compact clusters than in the OCS are produced. The maximum obstruction occurs when the colloidal particles are minority ($x>0.5$).

In model 2 the impurities are mobile monomeric particles. In this case the growth kinetics is significantly slowed down, resulting in extremely long simulations. For this reason we have done calculations for only one concentration, $\phi=0.01$, for molar fractions $x=0.1,0.2,0.3$, and 0.5, and the results are averaged over 50, 15, 10, and 6 simulations, respectively. The fractal dimension of the colloidal B clusters for this model is plotted as a function of the relative concentration ϕ_B in Fig. 2(a) (asterisks). Also plotted is the OCS (dotted line) and results for model 1 at $\phi=0.01$ (circles). Figure 2(b) shows the dependence of d_f on the molar fraction of impurities and a comparison to results in model 1. The fractal dimension is significantly lower than in both the OCS and model 1. This can be explained by the fact that the unaggregated fast mobile impurities develop a large *effective* volume that cannot be reached by the colloidal aggregates.

IV. AGGREGATION KINETICS

Experimentally, the mean number of clusters $N_c(t)$ and the weight-average cluster size $S_w(t)$ give enough information on the kinetics of aggregation. Whenever these two quantities show a power law behavior with time, then plots of the cluster distribution function $N_s(t)$ at different times collapse onto one master curve following the scaling equation $N_s(t)\sim S_w^{-2} f(s/S_w)$ [19]. This scaling is also found in numerical simulations of OCS DLCA [14]. In the scaling regime two dynamical exponents define the temporal change of the above quantities: $N_c(t)\sim t^{-z'}$ and $S_w(t)\sim t^z$.

For model 1 and model 2, Figs. 3 and 4 illustrate the time dependence of $N_c(t)$ and $S_w(t)$ at $\phi=0.01$ and at two values of the molar fraction of impurities. For model 1 the power law behavior extends for a long period of time whereas in model 2 it is one to two decades shorter and decreases further when the impurity concentration changes from $x=0.1$ to

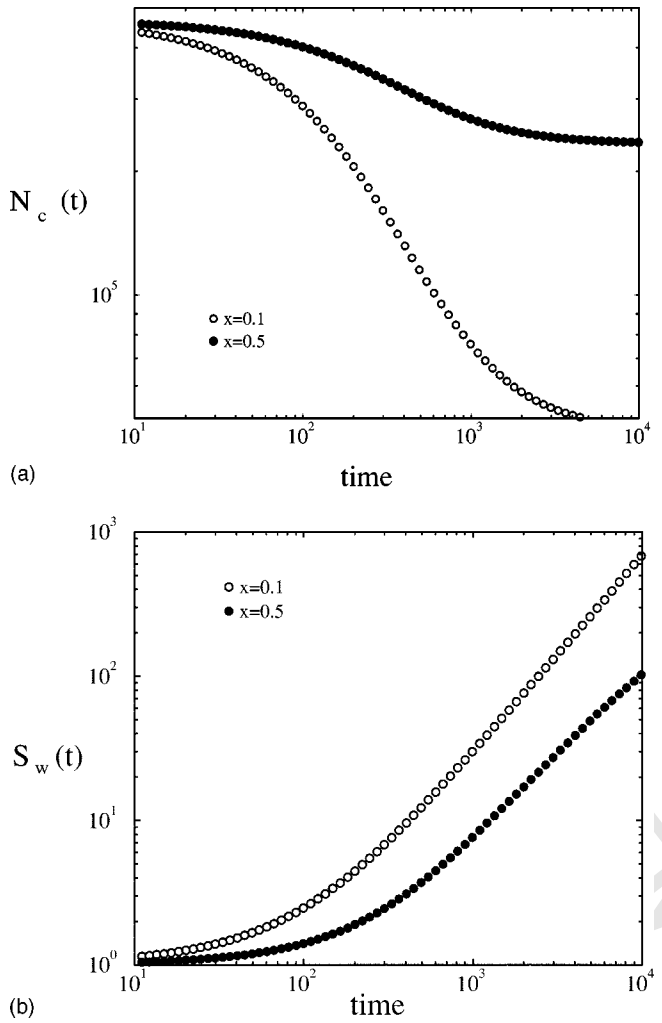

FIG. 4. Model 2: (a) Mean number of clusters $N_c(t)$ as a function of time. (b) Weight-average cluster size $S_w(t)$ as a function of time. Both plots are for $\phi=0.01$ and impurity molar fractions $x=0.1$ (circles) and $x=0.5$ (black dots).

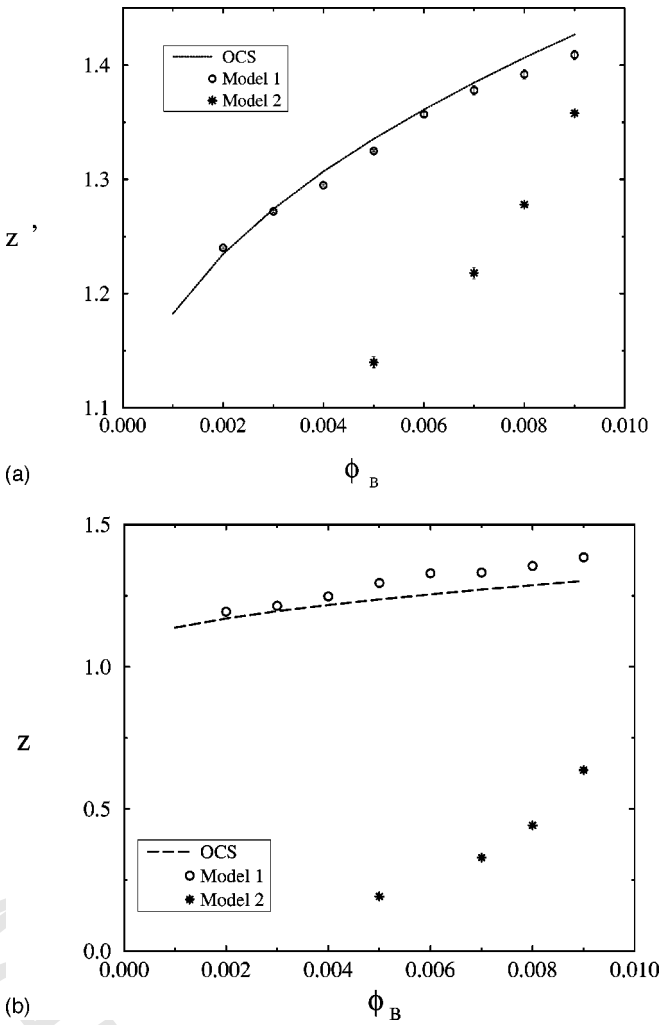

FIG. 5. (a) Exponent z' and (b) exponent z as a function of the relative concentration of the colloidal particles for model 1 and 2 at $\phi=0.01$.

$x=0.5$. The dynamical exponents z and z' were calculated from the slope of the linear time regime in the log-log plots of $S_w(t)$ and $N_c(t)$, respectively. Figures 5(a) and 5(b) show the dependence of these exponents on the relative concentration of the B particles, $\phi_B=(1-x)\phi$. As a comparison, the figure also displays the OCS results calculated from $z=1.067+3.088\phi^{0.547}$ and $z'=1.045+3.413\phi^{0.465}$ [14]. At low concentration, fractal impurities (model 1) have a slight effect on the kinetics while monomeric particles (model 2) dramatically affect the kinetics. Notice that for model 1, as ϕ_B increases, z' becomes slightly smaller than the OCS value. This effect is a consequence of the decreasing size of the impurity clusters with increasing concentration of the aggregating B particles. As a conclusion, the effect on the kinetics of small impurity clusters is more pronounced.

In the time regime where $N_c(t)$ and $S_w(t)$ follow a power law, it was possible to define a scaling equation for $N_s(t)$ in both models. Figure 6 illustrates the collapse onto one master curve of a typical case at $\phi=0.01$ and $x=0.5$.

V. GELATION AND PROPERTIES OF THE GEL

In the flocculation regime the system is composed of aggregates that are self-organized but still are not touching themselves. The finite size of the computational box leads to two possible final stages once the flocculation regime is continued in time. In one case the system terminates as one large cluster that has accrued all the particles in the bath but does not span the computational box. The second possibility is such that at the end of the simulation there is a spanning cluster, which we will refer to as the gel. A cluster spans when it spreads from edge to edge along the computational box as in percolation theory [12] and the time at which the cluster spans is called t_g or the gelation time. In the numerical simulations there is then a characteristic system concentration at which either one of the two cases is observed. This concentration is defined as the gelation (or percolation) threshold ϕ_g. For the OCS its dependence on the system size was proposed to follow $\phi_g \sim L^{D_f}/L^3 \sim L^{-(3-D_f)}$ [20], where $D_f \approx 1.8$ is the effective dimensionality of the simulated gel at infinite dilution. In the thermodynamic limit $L \to \infty$, the gelation threshold goes to zero, meaning that the system gels as predicted in the past [21].

Impurities could also affect the gelation threshold and other properties of the gel, especially at finite concentrations where we have seen large deviations of d_f from that of the one-component system. For model 1, the dependence of ϕ_g

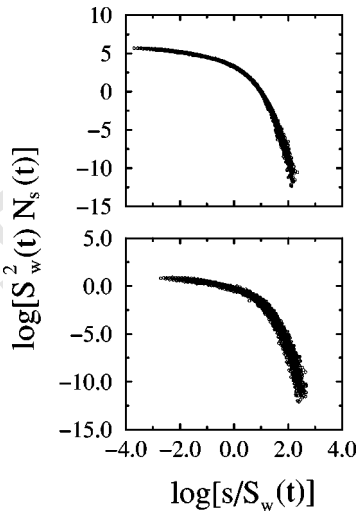

FIG. 6. Scaling of the cluster size distribution $N_s(t)$ in model 1 (top) and in model 2 (bottom) at $\phi=0.01$ and $x=0.5$.

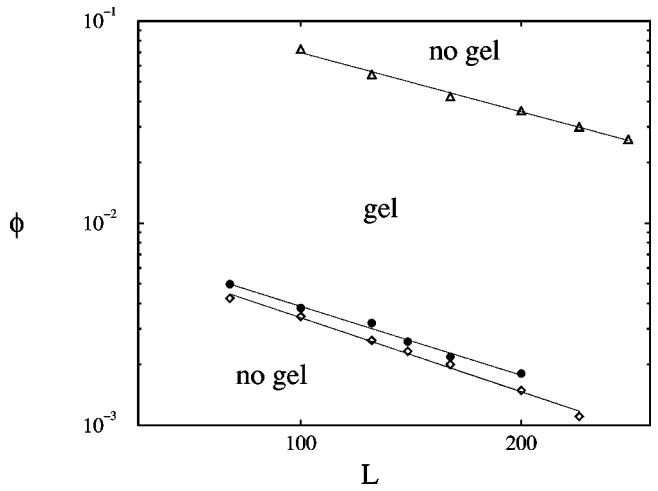

FIG. 7. Model 1: Phase portrait indicating the concentration boundary between the gelling and non-gelling regimes (triangles) for $x=0.5$. Also shown is the size dependence of the percolation threshold (diamonds). The size dependence of the percolation threshold in the one component system is given for comparison purposes (black dots).

on the system size L for a symmetric system $x=0.5$ was considered for sizes $L=80$, 100, 125, 140, 160, 200, and 240. For each L, the concentration is varied and 50 independent simulations for each concentration ϕ are performed. The threshold to gelation ϕ_g is defined as the concentration at which half of these simulations end up with a gel. Figure 7 is a log-log plot showing the dependence of ϕ_g on L (diamonds). We performed a similar study for the OCS and results are shown in the same figure (black dots). It is clear that the impurities (at $x=0.5$) have a somewhat lower threshold to gelation than the OCS and the slopes are not exactly equal. For the OCS, the slope of the data points is -1.13 ± 0.06 whereas in the impure system the slope is -1.22 ± 0.05. Using the relation between ϕ and L of Ref. [20] yields two effective dimensionalities of the simulated gel: $D_f \approx 1.87$ for the OCS and $D_f=1.78$ for the impure system (model 1 with $x=0.5$). This is in agreement with our previous results: fractal impurities reduce the fractal dimension.

To have a complete picture of the effect of impurities on gelation properties for model 1, additional higher concentration cases were considered. We believe that in this model there is a terminal finite concentration at which the impurity clusters fully inhibit the long range diffusion and growth of the colloidal clusters. In fact, at $\phi=0.05$ and $x=0.5$ the system does not gel for values of L larger than 150. Calculations similar to those described in the determination of the gelation threshold were used to identify this non-gelling region. For system sizes $L=100$, 120, 140, 160, 200, and 240, the concentration is changed and G, the gel fraction of B particles, is calculated from Eq. (1). Averages of G over 40 independent simulations are calculated for each ϕ at a given L. Subsequently these averages as a function of increasing ϕ are fitted by an exponential function to extract the limiting ϕ at which $G=0$. This process is repeated for every L and the results are plotted in Fig. 7 (triangles). As clearly seen, in the regime of finite concentrations there is a gelling to nongelling transition. Figure 7 represents a phase portrait of the system showing regions of gelation and nongelation for the aggregating system with mobile aggregating impurities, at a molar fraction $x=0.5$.

The obstruction to aggregation of the B colloidal particles was further investigated with the aid of the pair correlation function:

$$g_{BB}(r,t)=\frac{[\text{density of } BB \text{ pairs in } (r,r+\delta r)]}{(\text{averge density of } BB \text{ pairs})}. \quad (3)$$

This pair correlation function was calculated at three different aggregation times for a system inside the gelling regime zone of the phase portrait in Fig. 7 ($\phi=0.01$, $L=100$) and for another system in the nongelling regime ($\phi=0.1$, $L=100$). Equation (3) is the pair correlation function of B particles belonging to nonspanning clusters. Typical results for $g_{BB}(r,t)$ at $x=0.5$ are plotted in Fig. 8 for these two concentrations. Figure 8(a) illustrates the temporal behavior of the pair correlation function at a concentration in the gelling region of $\phi=0.01$ for $x=0.5$. The position of the minimum of this function gives a rough estimate of the average linear cluster size [18]. As time proceeds the colloidal clusters grow more extended and the linear cluster size increases, until the gel is formed. At this point the structure of $g_{BB}(r,t)$ is lost since one spanning cluster is present and the linear cluster size diverges. A similar behavior was observed at an impurity mole fraction of $x=0.8$. Figure 8(b) illustrates the temporal change of $g_{BB}(r,t)$ in the nongelling region ($\phi=0.1$), showing that the linear cluster size reaches a saturation value after a characteristic time. Small oscillations in $g_{BB}(r,t)$ are present, reflecting the incipient appearance of a local ordering of clusters which prevents the formation of a gel. For $x=0.8$, we have found that the impurities form a gel and the colloidal clusters are trapped in this gel exhibiting a local ordering [a second peak in $g_{BB}(r,t)$].

We have also studied the effect of monomeric impurities on gelation (model 2). For one system of size $L=100$, several values of the relative concentration ϕ_B of the B colloidal particles were chosen: 0.005, 0.01, 0.02, 0.03, and 0.04. For each ϕ_B value the number of impurities N_A is increased until

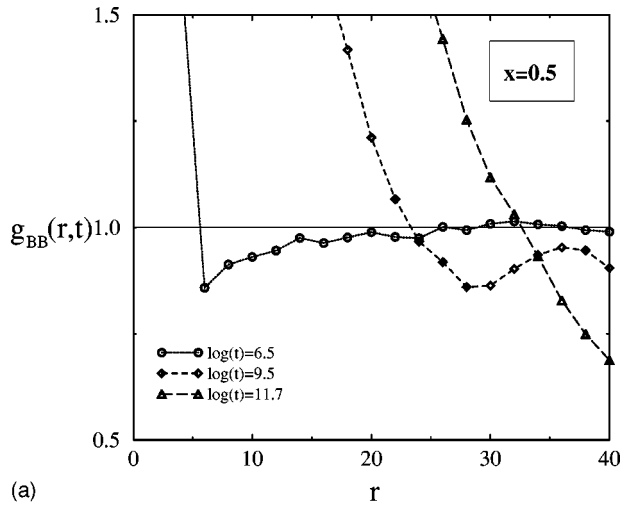

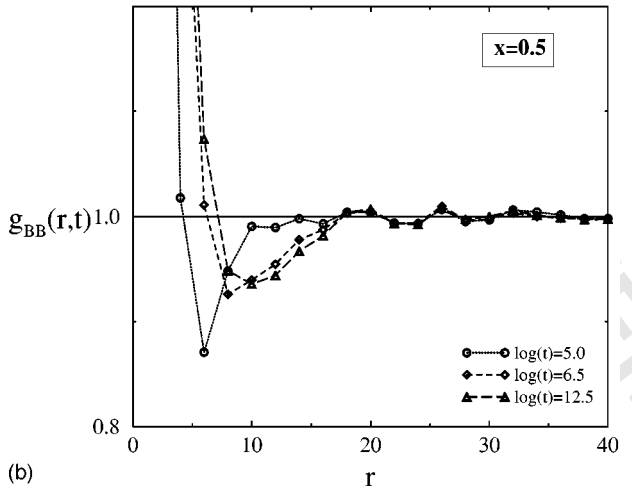

FIG. 8. Model 1: (a) Pair correlation function at three different times: $\ln(t)=6.5$ (circles), 9.5 (diamonds), and 11.7 (triangles) for a system in the gelling regime at $\phi=0.01$ and $x=0.5$. (b) The same function but now for the times $\ln(t)=5.0$ (circles), 6.5 (diamonds), and 12.5 (triangles) for a system in the nongelling regime at $\phi=0.1$ and $x=0.5$.

the system stops gelling. Results yield the phase portrait shown in Fig. 9 where points for $\phi_A = 0.0041$, 0.0073, 0.0115, 0.0185, and 0.0225 are at the boundary between the gelling and nongelling behavior. Due to the extremely long computational time involved in this type of simulation, only one run was performed for each case, taking a total of 57 hours of CPU time in a dedicated R10000 195 MHz processor for the full simulation. It is apparent from Fig. 9 that there is a boundary in the plane (ϕ_A,ϕ_B) between the gelling and nongelling regions. This portrait indicates that, when the relative concentration of the B particles is increased, there is a value of ϕ_A, consistent with a molar fraction of impurities x_c, above which gelation is fully blocked.

VI. CONCLUSION

We have shown in two different lattice models that mobile impurities affect the structure and the kinetics of a colloidal DLCA system. This effect is very strong when the impurities are unreactive (model 2) because these particles

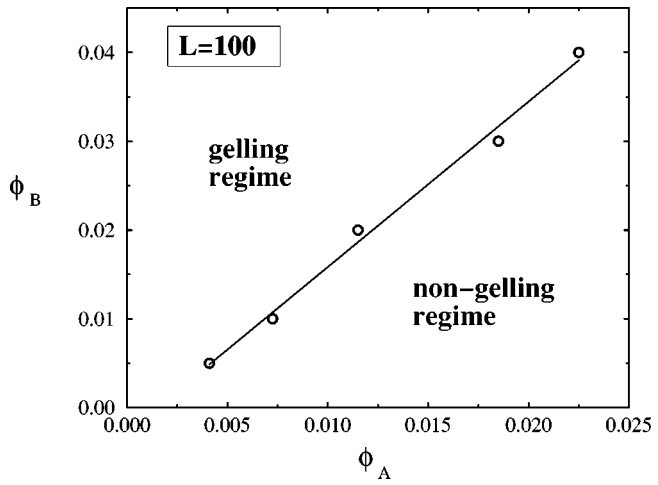

FIG. 9. Model 2: Phase portrait in the plane of the relative concentrations ϕ_A and ϕ_B, showing the gelling and nongelling regions.

move more frequently than the colloidal clusters and occupy a larger effective volume, such that the colloidal particles are constrained to form elongated aggregates and therefore their fractal dimension decreases. This is in agreement with the experimental result [8] that the storage modulus decreases monotonically when unreactive fillers are present. The aggregation kinetics in this impure system is dramatically slowed down, since the number of small obstacles prevents the large colloidal clusters from moving to form larger clusters. Furthermore, for a finite system there is indication that, with increasing concentration of the colloidal particles, there is a molar fraction of impurities x_c above which gelation is fully inhibited.

In the case of reacting impurities (model 1), their aggregated structure makes them less effective in blocking the aggregation of the colloidal particles and only at relatively large concentrations do they reduce the fractal dimension of the colloidal aggregates. In this process the kinetics is closer to that of the one-component system at equivalent concentrations. However, a nongelling region appears at high concentrations, where the impurity aggregates block the diffusion of the colloidal clusters, thus preventing further growth. The pair correlation function shows that the impurities keep the colloidal clusters apart, displaying a spatial local ordering. A word of caution should be said when trying to extrapolate this result to a system of clusters diffusing in the continuum, with the additional possibility of rotational diffusion. As we understand it, this hindrance to gelation occurs because the impurity clusters block the diffusion of the colloidal clusters that, in our model, occurs only by translational diffusion and by steps of one lattice spacing, which is of the order of the particle diameter. It might be possible that in an experimental system, with shorter step lengths and with the possibility of rotational diffusion by short angular steps, the clusters may disentangle and escape from the cages where they are trapped (formed by the impurity clusters). In this case, a disentangled cluster may find another one of the same species, and further growth would continue above the gelation point. A definitive proof of this scenario has to wait for the execution of very sophisticated computer simulations or for experimental results with the above features.

ACKNOWLEDGMENTS

E.B.B. acknowledges partial support for this work from the National Science Foundation through Grant No. CTS-9806321. A.E.G acknowledges partial support from CONACyT (Mexico) through Grant Nos. 3165-PE and E120.1381. A.AlS. is indebted to the Saudi Arabia government for financial support and to the Institue for Computational Sciences at George Mason University for generous support.

[1] H. FurediMilhofer and S. Sarig, Prog. Cryst. Growth Charact. Mater. **32**, 45 (1996).
[2] S. D. Durbin and G. Feher, Annu. Rev. Phys. Chem. **47**, 171 (1996).
[3] F. Rosenberger, P. G. Vekilov, M. Muschol, and B. R. Thomas, J. Cryst. Growth **168**, 1 (1996).
[4] M. Skouri, B. Lorber, R. Geige, J. P. Munch, and J. S. Candau, J. Cryst. Growth **152**, 209 (1995).
[5] M. J. Kositza, C. Bohne, P. Alexandridis, T. A. Hatton, and J. F. Holzwarth, Langmuir **15**, 322 (1999).
[6] P. Terech, G. Gebel, and R. Ramasseul, Langmuir **12**, 4321 (1996).
[7] J. B. Li, R. Miller, D. Vollhardt, and H. Mohwald, Thin Solid Films **329**, 84 (1998).
[8] T. van Vliet, Colloid Polym. Sci. **266**, 518 (1988).
[9] M. L. Anderson, C. A. Morris, R. M. Stroud, C. I. Merzbacher, and D. R. Rolison, Langmuir **15**, 674 (1999).
[10] N. Vandewalle and M. Ausloos, Phys. Rev. Lett. **77**, 510 (1996).
[11] K. Ivanova, Phys. Rev. B **58**, 1 (1998).
[12] D. Stauffer and A. Aharony, *Introduction to Percolation Theory* (Taylor and Francis, London, 1992).
[13] A. AlSunaidi, M. Lach-hab, A. E. González, and E. Blaisten-Barojas, Phys. Rev. E **61**, 550 (2000).
[14] M. Lach-hab, A. E. González, and E. Blaisten-Barojas, Phys. Rev. E **54**, 5456 (1996).
[15] M. J. Saxton, Biophys. J. **64**, 1053 (1993).
[16] B. B. Mandelbrot, H. Kaufman, A. Vespignani, I. Yekutieli, and C. H. Lam, Europhys. Lett. **29**, 599 (1995).
[17] D. Queiros-Conde, Phys. Rev. Lett. **78**, 4426 (1997).
[18] M. Lach-hab, A. E. González, and E. Blaisten-Barojas, Phys. Rev. E **57**, 4520 (1998).
[19] M. Broide and R. J. Cohen, Phys. Rev. Lett. **64**, 2026 (1990).
[20] A. Hasmy, E. Anglaret, M. Foret, J. Pelous, and R. Jullien, Phys. Rev. B **50**, 6006 (1994).
[21] M. Kolb and H. Hermann, J. Phys. A **18**, L435 (1985).